RSC Advances

ROYAL SOCIETY OF CHEMISTRY

www.rsc.org/advances

High-rate electrode material $2LiFePO_4 \cdot Li_3V_2(PO_4)_3$@carbon/graphene using the in-situ growing $Fe_4(VO_4)_4 \cdot 15H_2O$ precursor on the surface of graphite oxide

Bao Zhang, Hui Li, Jia-feng Zhang*

School of Metallurgy and Environment, Central South University, Changsha, Hunan, 410083, China

Abstract: $2LiFePO_4 \cdot Li_3V_2(PO_4)_3$@carbon/graphene (2LFP·LVP@C/G) as cathode material, based on in-situ growing $Fe_4(VO_4)_4 \cdot 15H_2O$ precursor on the surface of graphene oxide, was synthesized by solid-state process. The X-ray diffraction Rietveld refinement and Raman spectroscopy results indicated that multi-phase structural $2LiFePO_4 \cdot Li_3V_2(PO_4)_3$ with carbon/graphene coating was obtained. The morphology is characterized by HRTEM tests, which reveal well crystallized 2LFP·LVP@C/G with bridging graphene nanosheets, forming an effective three-dimensional conducting network. Compared with $2LiFePO_4 \cdot Li_3V_2(PO_4)_3$@carbon(2LFP·LVP@C), the electrochemical results demonstrate that the 2LFP·LVP@C/G electrode measured at 0.1C and 10C can deliver a high specific discharge capacity of 151.2 mAh g^{-1} and 125.4 mAh g^{-1}, respectively. and has a discharge capacity of 100.2mAh g^{-1} at -30℃ at 0.1C, indicating better rate capability and temperature property.

Keywords: $Fe_4(VO_4)_4 \cdot 15H_2O$/GO, $2LiFePO_4 \cdot Li_3V_2(PO_4)_3$@C/G, reduced graphene oxide

1 Introduction

Since Padhi et al.[1] firstly reported that lithium iron phosphate was a potential cathode for lithium ion batteries, many works had been devoted to preparing transition metal polyanion materials based on PO_4^{3-}, such as orthorhombic $LiMPO_4$(M = Fe, Mn, Co, Ni) [2,3] and monoclinic $Li_3M`_2(PO_4)_3$(M`=Fe, V)[4-5]. Olivine-type $LiFePO_4$ is one of the most promising cathode materials for the advantages of abundant resources, stable structures, high power density and nontrivial safety. However, $LiFePO_4$ has inherently poor electrical conductivity (1.8×10^{-9} S/cm) and ionic conductivity (10^{-16}~10^{-14}S/cm), which hinder its practical applications[6-7]. The presence of the tetrahedral poly-anion (PO_4^{3-}) with strong covalently-bond in the olivine structure

*Corresponding author: Jia-feng Zhang, E-mail: csuzjf@vip.163.com;Tel: +86-731-88877248

could provide a steady three-dimensional framework, thus retaining the excellent cycling performance and thermal stability for $Li_3V_2(PO_4)_3$ cathode materials[8]. Compared with $LiFePO_4$, monoclinic $Li_3V_2(PO_4)_3$ possesses superior electrical conductivity(2.4×10^{-7}S/cm) and ionic conductivity (10^{-9}~10^{-8}S cm^{-1}), belonging to the lithium high ionic conductors with NASCION structure, which enables Li ions to intercalate and deintercalate effortlessly[8-10]. Therefore, the ionic diffusivity of $LiFePO_4$ could be improved by incorporating with $Li_3V_2(PO_4)_3$ and the xLiFePO$_4$·yLi$_3$V$_2$(PO$_4$)$_3$ compound is a novel strategy for enhancing the electrochemical performance of $LiFePO_4$[11-31]. Many mixtures of $LiFePO_4$ and $Li_3V_2(PO_4)_3$ have been studied and delivered excellent rate performances[32,33], such as, 100 mAh g^{-1} at 10 C for 2 $LiFePO_4$/C-$Li_3V_2(PO_4)_3$/C[34], 116.8 mAh g^{-1} at 10 C for 3 $LiFePO_4$/C-$Li_3V_2(PO_4)_3$/C[35], 114 mAh g^{-1} at 10 C for 5 $LiFePO_4$-$Li_3V_2(PO_4)_3$[36] ,93.3 mAh g^{-1} at 10 C for 9 $LiFePO_4$/C-$Li_3V_2(PO_4)_3$/C[37] etc.

Recently, graphene, with one-atom thick layer in 2D structure[38], has been implemented as a new and promising electron conducting additive for cathode materials of LIBs. Graphene can offer an improved interfacial contact because of its superior conductivity, flexible structure, especially, high surface area (2630 m^2 g^{-1} of theoretical value)[39], which can form a 2D electron conducting network in cathode materials to increase electron conductivity[40]. Ding et al. reported $LiFePO_4$/graphene composites prepared through a co-precipitation method[41], and Zhou et al. synthesized graphene modified $LiFePO_4$ composites with excellent electrochemical properties by spray-drying and annealing processes[42]. Liu et al. prepared $Li_3V_2(PO_4)_3$/graphene composite with a high specific discharge capacity of 82 mAh g^{-1} at 50 C rate in the potential range of 3.0-4.3 V[43].

However, the interfacial interaction between cathode materials and graphene is inefficiency and graphene was difficult to be uniformly dispersed, which is led to quite limitation about the enhancement in electrical conductivity. Consequently, it remains necessary to develop an approach to construct effective graphene networks for fully utilizing its potential properties.

In this paper, a novel in-situ growing $Fe_4(VO_4)_4\cdot15H_2O$ precursor on the surface of graphite oxide are developed to a novel 3D hierarchical 2$LiFePO_4$·$Li_3V_2(PO_4)_3$@carbon/graphene (2LFP·LVP@C/G) composite cathode in situ for the first time. The composite showed enhanced electrochemical performance as cathode material for Li-ion battery compared with

$2LiFePO_4 \cdot Li_3V_2(PO_4)_3$@C(2LFP·LVP@C).

2 Experimental

The precursor $Fe_4(VO_4)_4 \cdot 15H_2O$/GO was prepared by ultrasonic-aided precipitation method. Firstly, Graphene oxide(GO) was prepared from graphite powder(Aldrich, powder, b20μm, synthetic) according to the method reported by Hummers[44]. Then, a 2M aqueous solution of $Fe(NO_3)_3 \cdot 9H_2O$ and GO(the weight ratio of GO to $Fe_4(VO_4)_4 \cdot 15H_2O$ was 10:90) were mixed in an ultrasonic-aided reaction vessel under vigorous stirring at 60℃ for 24h. Then, the desired amount of NH_4VO_3 was added drop wise under a continuous stirring. The molar ratio of Fe:V was 1:1. Meanwhile, $NH_3 \cdot H_2O$ was employed to adjust the pH of the reaction solution to 6. As we expected, a brown precipitate $Fe_4(VO_4)_4 \cdot xH_2O$/GO was spontaneously appeared, finally the precipitate was collected after washing by deionized water and dried in an oven at 80℃. The possible reaction may occur as follow:

$$V_4O_{12}^{4-} + 4Fe^{3+} + 8OH^- + 15H_2O + GO \rightarrow Fe_4(VO_4)_4 \cdot 15H_2O/GO$$

The 2LFP·LVP@C/G was prepared by mixing stoichiometric amounts of as-prepared $Fe_4(VO_4)_4 \cdot 15H_2O$/GO, LiH_2PO_4, oxalic acid and glucose in ethanol medium under high-energy ball milling for 5 h. The as-obtained powders were sintered in a horizontal quartz tube at 700℃ for 18h under a 5:95 hydrogen-argon atmosphere, then the 2LFP·LVP@C/G composites were finally obtained. The synthesis process for the 2LFP·LVP/G composites is schematically illustrated in Fig.1. Meanwhile, the material 2LFP·LVP@C was prepared via the same process without using Graphene oxide as precursor for comparison.

Structural and crystalline phase analyses of the products were taken from the powder X-ray diffraction (XRD, Rint-2000, Rigaku) using Cu Kα. Residual carbon content in both samples was determined by a carbon sulfur analyzer (CS600,LECO, US). The samples were observed by SEM (JEOL, JSM-5600LV) and a Tecnai G12 transmission electron microscope (TEM). Thermo gravimetric (TG) analysis of the precursor was measured on a SDT Q600 TG-DTA apparatus at the temperature between 25℃ and 800℃ with a heating rate of $10℃ min^{-1}$ under air flow. Raman

scattering (RS) spectra were recorded on a HORIBA Scientific LabRAM HR Raman spectrometer system.

The electrochemical characterizations were performed using CR2025 coin-type cell. Typical positive electrode loadings were in the range of 2-2.5 mg cm^{-2}, and an electrode diameter of 14 mm was used. For positive electrode fabrication, the prepared powders were mixed with 10% of carbon black and 10% of polyvinylidene fluoride in N-methyl pyrrolidinone until slurry was obtained. And then, the blended slurries were pasted onto an aluminum current collector, and the electrode was dried at 120℃for 12 h in the air. The test cell consisted of the positive electrode and lithium foil negative electrode separated by a porous polypropylene film, and 1.0mol L^{-1} (0.9$LiBF_4$-0.1LiBOB) in PC-EC-EMC(1:1:1 in volume) was used as the electrolyte. The assembly of the cells was carried out in a dry Ar-filled glove box. Electrochemical tests were carried out using an automatic galvanostatic charge-discharge unit, NEWARE battery cycler, between 2.5V and 4.5V versus Li/Li^+ electrode at room temperature. Cyclic voltammograms(CV) were measured on a LK9805 electrochemical interface at a scanning rate of 0.1 mV s^{-1}. Electrochemical impedance spectroscopy(EIS) was conducted using an electrochemical analyzer(Zahner) at frequencies from 100kHz to 10mHz with a perturbation amplitude.

3 Results and discussion

The TG/DTA curves of $Fe_4(VO_4)_4 \cdot 15H_2O$/GO compounds are shown in Fig. 2a. It can be seen that the main weight loss is up to 11.5% from 25℃ to 370℃ in the TG curve and two endothermic peaks occur at 113℃ and 369℃ in the DTA curve, indicating that the number of crystal water in the $Fe_4(VO_4)_4 \cdot 15H_2O$/GO is 15. Then, an exothermic peak appeared in the DTA curve at 409℃ is ascribe to loss of GO(5.5%). Meanwhile, a litter exothermic peak appeared in the DTA curve at 462℃ corresponds to the decomposition of $Fe_4(VO_4)_4$ and the crystal transformation of $FeVO_4$. The XRD patterns of $Fe_4(VO_4)_4$ and $FeVO_4$ are shown in Fig. 2b . The morphology of $Fe_4(VO_4)_4 \cdot 15H_2O$/GO was characterized by SEM. As we can see from Fig. 2c, the particles of $Fe_4(VO_4)_4 \cdot 15H_2O$ grow on the surfaces of graphene oxide. Additionally, the Fe/V mole ratio of $Fe_4(VO_4)_4 \cdot 15H_2O$ is 1.002 based on analysis of chemical titration, which confirms that the as prepared brown precipitate is $Fe_4(VO_4)_4 \cdot 15H_2O$/GO.

The XRD patterns of 2LFP·LVP@C/G and 2LFP·LVP@C are shown in Fig. 3, it indicates that two different $2LiFePO_4 \cdot Li_3V_2(PO_4)_3$ composites are all composed of orthorhombic $LiFePO_4$(space group Pnmb, PDF #83-20921) and monoclinic $Li_3V_2(PO_4)_3$ (space group $P2_1/n$, PDF #78-1465) phases without other impurities. There is no evidence of diffraction peaks for the carbon in all samples, indicating graphene. The Rietveld refinement result indicates the sample consists of two phases: LFP [46.5% w/w] and LVP [53.5% w/w]. The residual carbon contents of 2LFP·LVP@C/G and 2LFP·LVP@C measured using Carbon Sulfur Analysis are 13.7 wt % and 14.0 wt %, respectively. The weight ratio of amorphous carbon to graphene in 2LFP·LVP@C/G composite is calculated to be 3:1.

The TEM images of 2LFP·LVP@C/G is shown in Fig.4. It can be seen from Fig. 4a that 2LFP·LVP@C/G nanoparticles with the size of about 180 nm are anchored on the surface of graphene sheets, which have tight contact surface with flexible graphene sheets. The Fig. 4b reflects the HRTEM images of 2LFP·LVP@C/G. It is found that there are two kinds of lattice fringes in the composite, one is the lattice fringe of $LiFePO_4$ with an interplanar spacing of 0.278 nm, which corresponds to the (0 3 1) lattice planes, and the other is lattice fringe of $Li_3V_2(PO_4)_3$ with an interplanar spacing of 0.238 nm, which corresponds to the (1 4 2) lattice plane. The results imply that $LiFePO_4$ unit cell, $Li_3V_2(PO_4)_3$ unit cell and $2LiFePO_4 \cdot Li_3V_2(PO_4)_3$ unit cell coexist in the composite materials.

Fig. 5a shows the first charge/discharge curves of the different 2LFP·LVP@C samples at 0.1C rate. At such rate, 2LFP·LVP@C/G exhibited the optimal initial discharge capacity of $152.1mAhg^{-1}$ with a average voltage of 3.66V over a voltage of 2.5-4.5V, while 2LFP·LVP@C are only $130.7mAhg^{-1}$ with a average voltage of 3.58V over a voltage of 2.5-4.5V, indicating unique structure (partices growth on grapheme) has positive effects on the electrochemical performances. To the best of our knowledge, the graphene oxide consists of sufficient oxygen containing groups, such as carboxyl, hydroxyl, and epoxide groups[45], which provide sites for the adsorption of Fe^{3+} and nanoparticles nucleation to achieve uniform $Fe_4(VO_4)_4$ on the surface of graphene oxide. The

resulting nanoparticles could be bonded to the partial GO by Fe-O-C bonds at the remaining oxygen sites and by van der Waals interactions with the aromatic regions of the partial GO.

Fig. 5b shows cycle performance of 2LFP·LVP@C/G and 2LFP·LVP@C at different rates. The cells were cycled at different rates from 0.1C to 10C and then returned to 0.1C (10 cycles for each rate). It can be clearly seen that the discharge capacity of both samples gradually decreases with increasing rate because of the increased polarization and the decreased utilization of active materials at high current density. However, the highly stable reversible capacity of 125.4mAh g^{-1} has been obtained at 10 C with a average voltage of 3.50V over a voltage of 2.5-4.5V for 2LFP·LVP@C/G compared with only a value of 44.5 mAh g^{-1} for LFP·LVP@C. Moreover, it is remarkable that the 2LFP·LVP@C/G electrode still remains a good discharge capacity of 151.2 mAh g^{-1} at 0.1 C after 50 cycles, which shows better electrochemical performance.

The rate capability of 2LFP·LVP@C/G at different rates is presented in Fig.5c. The discharge capacities of the composites at the different rate of 0.1C, 1C, 2C, 5C and 10C are 152.1mAh g^{-1}, 142.4mAh g^{-1}, 136.6mAh g^{-1}, 131.7mAh g^{-1} and 126.2mAh g^{-1}, respectively. Fig.5d shows high and low temperature property of 2LFP·LVP@C/G. The thermal and chemical stabilities of graphene guarantee the safety when it is used in harsh environments. The discharge capacities of the composites at the temperature of 55℃, -10℃, -20℃ and -30℃ are 167.5mAh g^{-1}, 128.8mAh g^{-1}, 116.0mAh g^{-1} and 100.2mAh g^{-1}, respectively. The excellent performance of material 2LFP·LVP@C/G at high rate and extreme temperature could be attributed to 3D electron conducting network formed in the samples when precursors were mixed properly, which may increases electron conductivity so as to enhance rate capability and cycle ability.

The cyclic voltammetry curves of the different composites at a scan rate of 0.1 mV s^{-1} between 2.5-4.5V are presented in Fig. 6a. The cathodic and anodic peaks indicate the potential difference between the oxidation and reduction processes, which was ascribed to the lithium extraction and insertion, respectively. The oxidation curve in the 2LFP·LVP@C/G consist of 4 anodic peaks at approximately 3.519V, 3.617V, 3.695V and 4.114V, while the reduction curve include corresponding cathodic peaks at 3.339V, 3.549V, 3.627V and 4.007V. Compared with 2LFP·LVP@C, it is noticeable that 2LFP·LVP@C/G exhibits more symmetrical and shaper of peaks and the voltage gap between the redox peaks is obviously much smaller, which indicate that

2LFP·LVP@C/G presents much better reversibility for Li^+ extraction/insertion. These results are in accordance with the charge and discharge curves obtained previously.

Fig.6b shows the electrochemical impedance spectroscopy of different composites after the first charge-discharge rate at 0.1C. Each spectrum consists of a semicircle in the high-frequency region and a straight line in the low-frequency region. The depressed semicircle in high-frequency region was attributed to the charge-transfer resistance (R_{ct}) of the electrochemical reaction while the straight line was related to the diffusion-controlled Warburg impedance. It clearly shows that 2LFP·LVP@C/G exhibits a smaller semicircle than that of 2LFP·LVP@C, which indicates that reduced graphene oxide reduces charge transfer resistance and thus improves the electronic conductivity.

Raman spectroscopy has been recognized as one of the most sensitive tools for studying the structural properties of carbonaceous materials , and the result of the 2LFP·LVP@C/G composite material is shown in Fig. 6c. Two broad bands were detected at around 1586 cm^{-1} and 1358 cm^{-1} in the spectrum, which are ascribed to D band and G band, respectively. As D band is a breathing mode of *k*-point phonons of A1g symmetry and G band is usually assigned to E2g phonon of C sp^2 hybridized atoms [46], the sp^3/sp^2 bond quantity in material can be estimated by measuring the ratio of D and G band intensities I_D/I_G. This helps to evaluate the amount of graphene relative to other carbon materials, as it is known that carbon atoms in graphene are sp^2 hybridized. Compared with the I_D/I_G ratio of 0.898 for 2LFP·LVP@C, the 2LFP·LVP@C/G displays a lower ratio of 0.827, indicating that the presence of graphene in 2LFP·LVP@C/G. Most of the studies suggest that lower I_D/I_G ratios provide higher cathode discharge capacity at high discharge rates[47-50].

The excellent electrochemical performance of the composites may be due to the tightly contact between 2LFP·LVP@C and graphene. From the view of synergy effects, the resultant composite is not merely the sum of 2LFP·LVP@C and graphene, but rather a new material with new functionalities and properties. On the one hand, 2LFP·LVP@C anchored on grapheme suppress the agglomeration and restacking of graphene that increase the available surface area of

the grapheme, accompanied with high electrochemical activity. On the other hand, as a support, graphene can induce nucleation, growth and formation of 2LFP·LVP@C, which is uniform dispersion and controlled morphology on the surface of graphene with high chemical functionality. Therefore, 2LFP·LVP@C/G can form an excellent integrated structure with a 3D electron conductive net work.

4 Conclusion

In summary, a novel 3D hierarchical 2LFP·LVP@C/G Composite cathode were synthesized via conventional solid-state method with the home-made $Fe_4(VO_4)_4 \cdot 15H_2O$/GO precursor. Compared with 2LFP·LVP@C, 2LFP·LVP@C/G is more favorable for electron migration because of synergy effects, which indicate predominant electrochemical performance. The discharge capacities of 2LFP·LVP@C/G at the rate of 0.1C, 1C, 2C, 5C and 10C are 152.1mAh g^{-1}, 142.4mAh g^{-1}, 136.6mAh g^{-1}, 131.7mAh g^{-1} and 126.2mAh g^{-1}, respectively, while the discharge capacities at 0.1C with the temperature of 55℃, -10℃, -20℃ and -30℃ are 167.5mAhg^{-1}, 128.8mAh g^{-1}, 116.0mAh g^{-1} and 100.2mAh g^{-1}, respectively. The present work demonstrates that graphene incorporation is an efficient approach for $2LiFePO_4 \cdot Li_3V_2(PO_4)_3$ to improve the electrochemical performance.

Acknowledgment

We gratefully acknowledge the financial support for this work of the National Natural Science Foundation of China under grant number 51402365, and China Postdoctoral Science Foundation (2014M560651).

References

[1] A.K. Padhi, K.S. Nanjundaswamy, J.B. Goodenough. J. Electrochem. Soc. 144(1997)1188-1194.

[2] C. Delacourt, P. Poizot, M. Morcrette, J.M. Tarascon, C. Masquelier, Chem. Mater. 16 (2004) 93.

[3] X.L. Wu, L.Y. Jiang, F.F. Cao, Y.G. Guo, L.J. Wan, Adv. Mater. 21(2009) 2710.

[4] M.M. Ren, Z. Zhou, Y.Z. Li, X.P. Gao, J. Yan, J. Power Sources 162(2006)1357.

[5] M.Y. Saidi, J. Barker, H. Huang, J.L. Sowyer, G. Adamson, J. Power Sources 119-121

(2003)266.

[6] B.L. Ellis, K.T. Lee, L.F. Nazar, Chem. Mater. 22 (2010) 691-714.

[7] S. Ferrari, R.L. Lavall, D. Capsoni, E. Quartarone, A. Magistris, P. Mustarelli, P.Canton, J. Phys. Chem. C 114(2010)12598-12603.

[8] H. Huang, S.C. Yin, T. Kerr, N. Taylor, L.F. Nazar, Adv. Mater. 14 (2002)1525.

[9] S.C. Yin, H. Grondey, P. Strobel, H. Huang, L.F. Nazar, J. Am. Chem. Soc. 125(2003)326-327.

[10] G. Yang, H.D. Liu, H.M. Ji, Z.Z. Chen, X.F. Jiang, Electrochim. Acta 55(2010)2951-2957.

[11] F. Omenya, N.A. Chernova, S. Upreti, P.Y. Zavalij, K.W. Nam, X.Q. Yang, M.S. Whittingham, Chem. Mater. 23 (2011) 4733-4740.

[12] L.L. Zhang, G. Liang, A. Ignatov, M.C.Croft, X.Q. Xiong, I.M. Hung, Y.H. Huang, X.L. Hu,W.X. Zhang, Y.L. Peng, J. Phys. Chem. C 115 (2011) 13520-13527.

[13] M.R. Yang, W.H. Ke, S.H. Wu, J. Power Sources 165 (2007) 646-650.

[14] L.N. Wang, Z.C. Li, H.J. Xu, K.L. Zhang, J. Phys. Chem. C 112 (2008) 308-312.

[15] S.K. Zhong, L. Wu, J.Q. Liu, Electrochim. Acta 74 (2012) 8-15.

[16] Y. Guo, Y.D. Huang, D.Z. Jia, X.C. Wang, N. Sharma, Z.P. Guo, X.C. Tang, J. Power Sources 246(2014)912-917.

[17] J.F. Zhang, C. Shen, B. Zhang, J.C. Zheng, C.L. Peng, X.W. Wang, H. Li, X.B. Yuan, G.M. Chen, J. Power Sources 267 (2014) 227-234.

[18] H. Tang, X.D. Guo, B.H. Zhong, H. Liu, Y. Tang, R. Xu, L.Y. Li, J. Solid State Electrochem. 16 (2012) 1537-1543.

[19] J.C. Zheng, X.H. Li, Z.X. Wang, J.H. Li, L.J. Li, L. Wu, H.J. Guo, Ionics 15 (2009) 753-759.

[20] X.J. Chen, G.S. Cao, X.B. Zhao, J.P. Tu, T.J. Zhu, J. Alloys Compd. 463 (2008)385-389.

[21] J.Y. Xiang, J.P. Tu, L. Zhang, X.L. Wang, Y. Zhou, Y.Q. Qiao, Y. Lu, J. Power Sources 195 (2010) 8331-8335.

[22] B. Zhang, J.C. Zheng, Z.H. Yang, Ionics 17 (2011) 859-862.

[23] S.K. Zhong, L. Wu, J.C. Zheng, J.Q. Liu, Powder Technol. 219 (2012) 45-48.

[24] J. Hong, X.L. Wang, Q. Wang, F. Omenya, N.A. Chernova, M.S. Whittingham, J. Graetz, J. Phys. Chem. C 116 (2012) 20787-20793.

[25] H. Lin, Y.W. Wen, C.X. Zhang, L.L. Zhang, Y.H. Huang, B. Shan, R. Chen, Solid State

Commun. 152 (2012) 999-1003.

[26] X.P. Zhang, H.J. Guo, X.H. Li, Z.X. Wang, L. Wu, Solid State Ionics 212 (2012) 106-111.

[27] N. Hua, C.Y. Wang, X.Y. Kang, T. Wumair, Y. Han, J. Alloys Compd. 503 (2010)204-208.

[28] G. Yang, C.Y. Jiang, X.M. He, J.R. Ying, F.P. Cai, Ionics 18 (2012)59-64.

[29] J.C. Zheng, X.H. Li, Z.X. Wang, J.H. Li, L. Wu, L.J. Li, H.J. Guo, Acta Physico-Chimica Sinica, 25 (2009) 1916-1920.

[30] J.C. Zheng, X.H. Li, Z.X. Wang, J.H. Li, L.J. Li, L. Wu, H.J. Guo, Ionics, 15 (2009) 753-759.

[31] G. Yang, C.Y. Jiang, X.M. He, J.R. Ying, J. Gao, Ionics, 19 (2013) 1247-1253.

[32] F. Yu, L. Zhang, Y. Li, Y. An, M. Zhu, B. Dai, RSC Advances, 4 (2014) 54576-54602.

[33] F. Yu, P. QI, Y. An, G. Wang, L. Xia, M. Zhu, B. Dai, Energy Technology, (2015).

[34] M.R. Yang, W.H. Ke, S.H. Wu, J. Power Sources, 165 (2007) 646-650.

[35] L. Wu, J.J. Lu, S.K. Zhong, Journal of Solid State Electrochemistry, 17 (2013) 2235-2241.

[36]J.C. Zheng, X.H. Li, Z.X. Wang, D.M. Qin, H.J. Guo, W.J. Peng, J. Inorg. Mater., 24 (2009) 143-146.

[37] Z.P. Ma, G.J. Shao, X. Wang, J.J. Song, G.L. Wang, Ionics, 19 (2013) 1861-1866.

[38] K.S. Novoselov, A.K. Geim, S.V. Morozov, D. Jiang, Y. Zhang, S.V. Dubonos, I.V. Grigorieva, A.A. Firsov, Science 306 (2004) 666.

[39] A. Peigney, C. Laurent, E. Flahaut, R.R. Bacsa, A. Rousset, Carbon 39 (2001) 507-514.

[40] Kucinskis, G. Bajars, G.Kleperis, J. Power Sources 240 (2013) 66-79.

[41] Y. Ding, Y. Jiang, F. Xu, J. Yin, H. Ren, Q. Zhuo, Electrochem. Commun. 12 (2010) 10-13.

[42] X.F. Zhou, F. Wang, Y.M. Zhu, Z.P. Liu, J. Mater. Chem 21 (2011) 3353-3358.

[43] H.D. Liu, P. Gao, J.H. Fang, G. Yang, Chem. Commun. 47 (2011)9110.

[44] W.S. Hummers, R.E. Offeman, J. Am. Chem. Soc. 80 (1958) 1339.

[45] X.Y. Yang, X.Y. Zhang, Y.F. Ma, Y. Huang, Y.S. Wang, Y.S. Chen, J. Mater. Chem 19(2009)271.

[46] Z. Luo, T. Yu, J. Shang, Y. Wang, S. Lim, L. Liu, G.G. Gurzadyan, Z. Shen, J. Lin, Adv. Funct.

Mater. 21 (2011) 911.

[47] J. Yang, J. Wang, D. Wang, X. Li, D. Geng, G. Liang, M. Gauthier, R. Li, X. Sun, J. Power Sources 208 (2012) 340.

[48] X. Zhou, F. Wang, Y. Zhu, Z. Liu, J. Mater. Chem. 21 (2011) 3353.

[49] O. Toprakci, H.A.K. Toprakci, L. Ji, Z. Lin, R. Gu, X. Zhang, J. Renew. Sustain. Energy 4 (2012) 013121.

[50] M.M. Doeff, J.D. Wilcox, R. Kostecki, G. Lau, J. Power Sources 163 (2006) 180.

Figure captions

Fig. 1 Illustration of the preparation process of the 2LFP·LVP@C/G composites.

Fig.2 (a)TG-DTA curves of $Fe_4(VO_4)_4 \cdot 15H_2O$/GO. (b)XRD patterns of$Fe_4(VO_4)_4$ and $FeVO_4$.(c) SEM images of $Fe_4(VO_4)_4 \cdot 15H_2O$/GO.

Fig.3 (a)XRD patterns of 2LFP·LVP@C/G and 2LFP·LVP@C.(b)Rietveld refinement performed with X-ray diffraction pattern of 2LFP·LVP@C/G.

Fig.4 (a) TEM image of 2LFP·LVP@C/G particles, (b)Corresponding HRTEM images from the marked region I.

Fig.5 (a)Charge-discharge curves performance of 2LFP·LVP@C@C/G and 2LFP·LVP@C at 1C rate. (b)Cycle performance of 2LFP·LVP@C@C/G and 2LFP·LVP@C at different rate. (c) Rate performances of 2LFP·LVP@C/G. (d)Charge-discharge curves performance of 2LFP·LVP@C/G at different temperature for 0.1 C rate.

Fig.6 Cyclic voltammetry profiles of the 2LFP·LVP@C/G and 2LFP·LVP@C .

Fig.7 Electrochemical impedance spectroscopy of 2LFP·LVP@C/G and 2LFP·LVP@C.

Fig.8 Raman spectra of 2LFP·LVP@C/G and 2LFP·LVP@C.

Fig.1

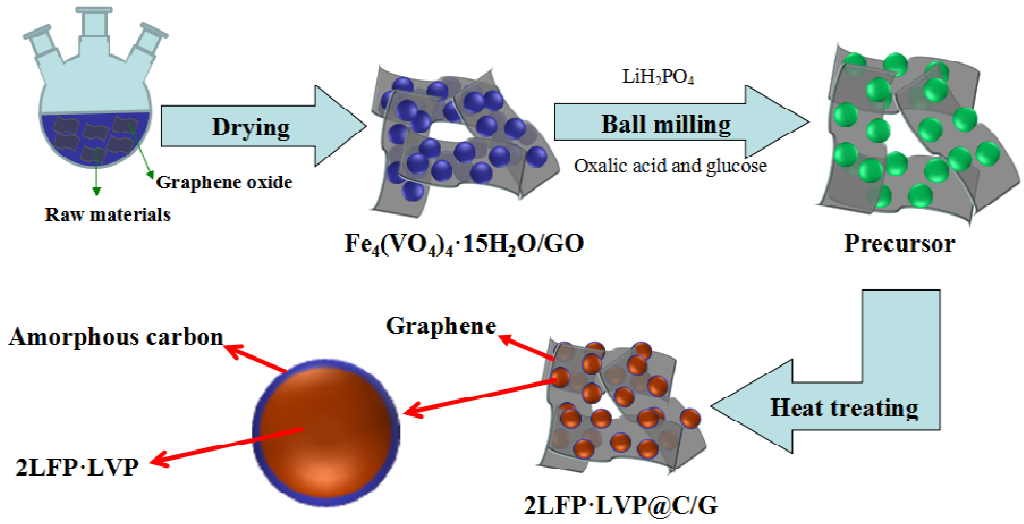

Fig. 2

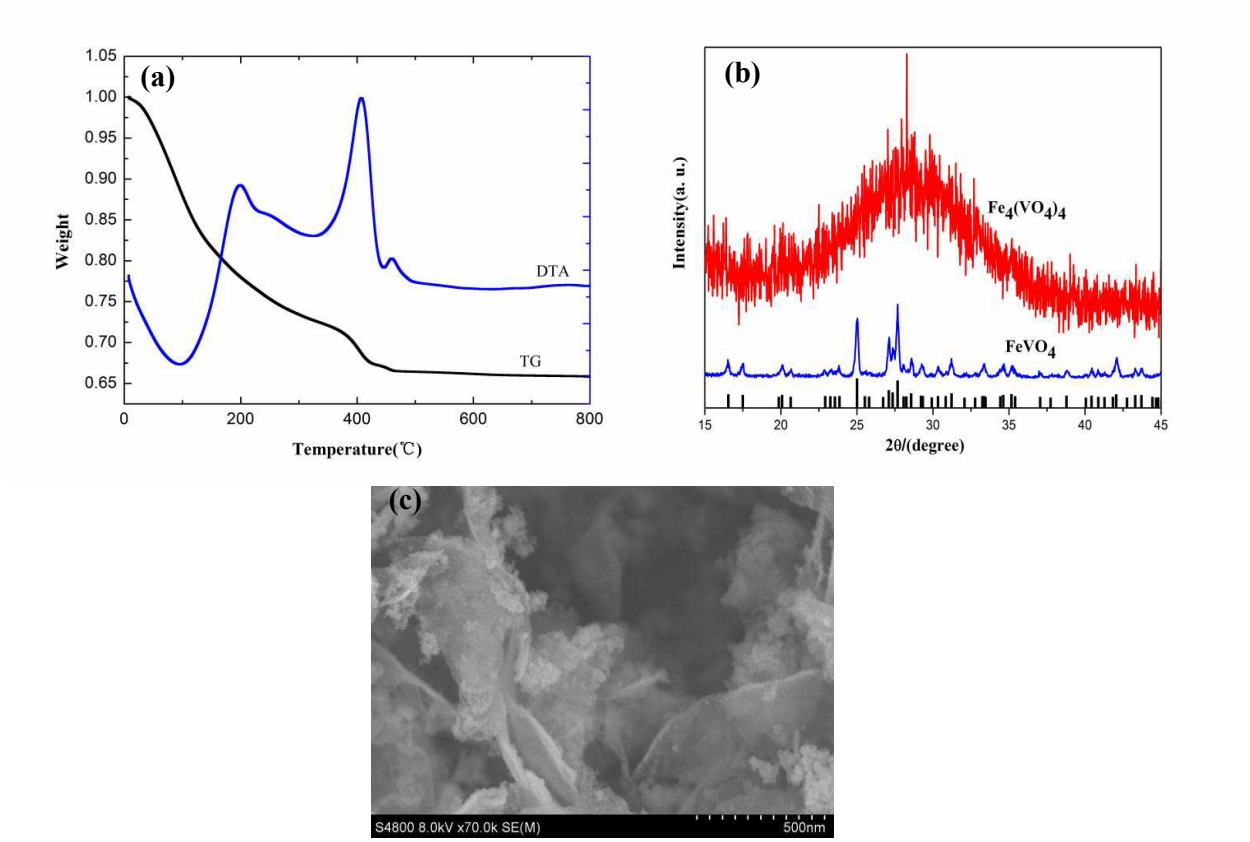

Fig. 3

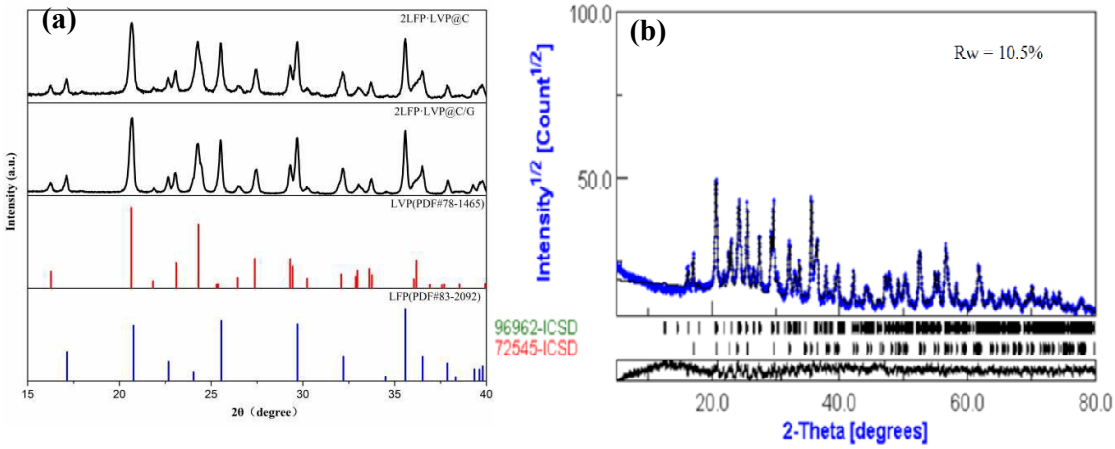

Fig. 4

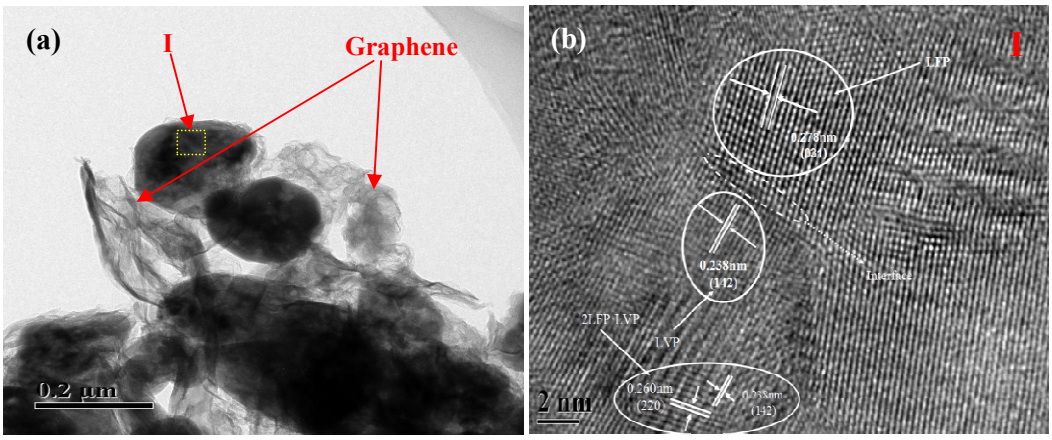

Fig.5

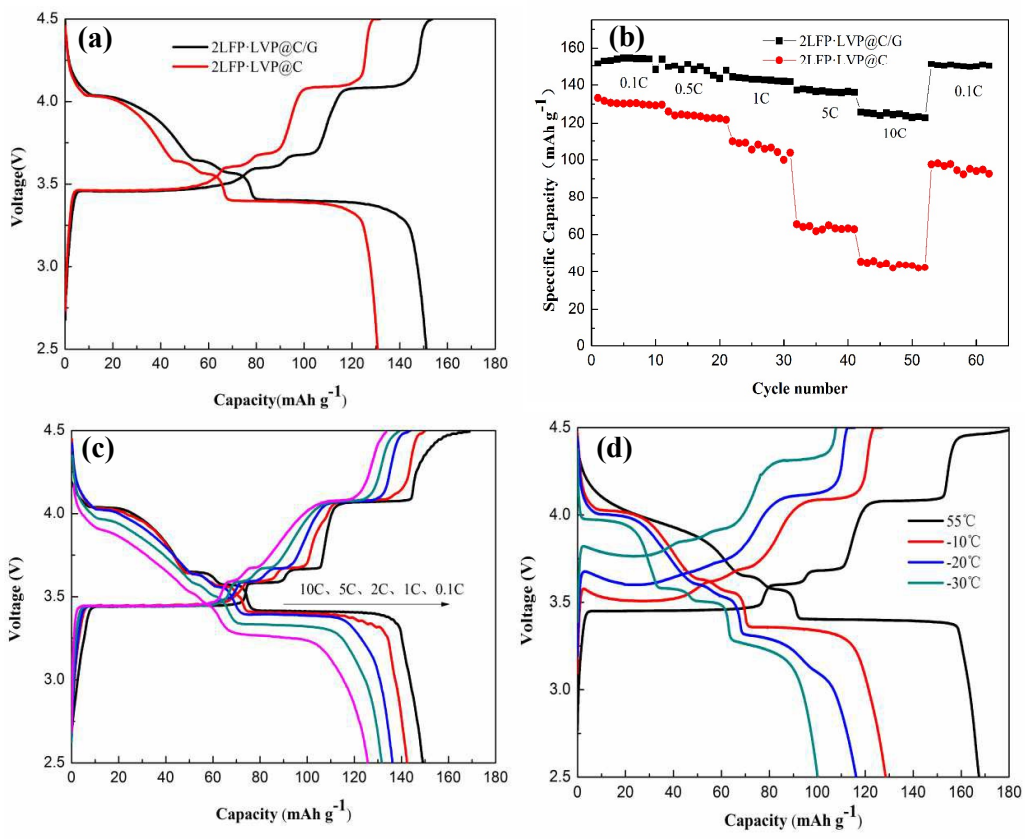

Fig.6